A METHOD FOR ANALYSIS OF PERFORMANCE OF THE SINGLE-PHASE RELUCTANCE MOTOR

By

LEONARD C. ADAMS

Bachelor of Electrical Engineering

Clemson Agricultural College

Clemson, South Carolina

1943

Submitted to the Faculty of the Graduate School of
the Oklahoma Agricultural and Mechanical College
in Partial Fulfillment of the Requirements
for the Degree of
MASTER OF SCIENCE

1950

A METHOD FOR ANALYSIS OF PERFORMANCE OF THE SINGLE-PHASE RELUCTANCE MOTOR

LEONARD C. ADAMS

MASTER OF SCIENCE

1950

THESIS AND ABSTRACT APPROVED:

Oliver F. Ellenberger
Thesis Adviser

Q. Naeter
Faculty Representative

R. E. McTeach
Dean of the Graduate School

PREFACE

If it cannot be said that research in the small motor field is interesting it may certainly be said that it is challenging. The least explored realms are invariably the most challenging, and one has but to institute a search for technical literature dealing with alternating-current motors of one-fiftieth horsepower or less to discover a relatively unexplored region.

This work presents the results of research in an attempt to analyze the principle of operation and performance of a single-phase reluctance motor rated at 1/100 horsepower. Since most of the findings discussed herein are based upon a study of this machine it seems well to describe it here.

The motor was manufactured by the Robbins and Meyers Corporation and assigned serial number 0589291ZA. It operates from a 115-volt, single-phase line delivering rated load at .43 amperes. It is a four-pole machine having two coils per pole on both the starting and main windings. Total weight of the motor is 7.1 lbs. It operates at a constant speed of 1800 rpm rendering it practical for such applications as turn-table drive, timer-motor, and recording-instrument drive.

This entire study is concentrated on the operating characteristics between no-load and 160% load. Chapters I and II present a qualitative analysis of the electric and magnetic fundamentals responsible for the operation of the machine as a motor. The fundamentals brought out in these chapters also provide a basis for explanation of performance as analyzed in Chapter III. In Chapter III a method of performance calculation

based upon complete test data is developed and demonstrated. The final chapter presents an alternate and less complicated method of making some of the performance calculations.

Explanation of the method of starting the motor has not been included in this thesis. To appease the curiosity of those interested in that aspect of the problem it may be stated that the rotor has a squirrel-cage winding, and the machine starts and runs up to a high percentage of synchronous speed as an induction motor. As a matter of fact, practical reluctance motor designs have been worked out by milling flats on a normal squirrel-cage induction motor.

It is hoped that this thesis will serve as a stepping-stone into the field of research dealing with the prediction of performance of miniature reluctance motors.

ACKNOWLEDGEMENT

The writer wishes to express his sincere appreciation to Professor C. F. Cameron for his many helpful suggestions and careful scrutiny of this material.

TABLE OF CONTENTS

CHAPTER I

Theory of Operation of the Reluctance Motor

PART I

Motor Circuits, Electric and Magnetic

The reluctance motor, as a type, may be referred to as a synchronous motor. This classification is justified by the fact that the machine operates throughout its entire load range at the synchronous speed of the stator field. It is peculiar to synchronous motors in general in that no direct current source of energy is required. In short, perhaps the easiest way to conceive of the reluctance motor is to imagine a conventional salient-pole synchronous motor operating at no-load and with the field circuit open. It is a well known fact that such a machine will continue to rotate and will even drive light loads. That motor power is available with open field may be explained from a consideration of the vector diagram[1] representing conditions in the salient-pole machine.

Refer to Figure I-1. The following table identifies the several vectors of the figure.

TABLE I

E_o - Developed e.m.f. due to total flux.

I_a - Total armature current.

I_q - Component of I_a along the quadrature axis.

I_d - Component of I_a along the direct axis.

R_e - Armature equivalent resistance.

---

[1] Thomas C. McFarland, Alternating Current Machines, p. 323.

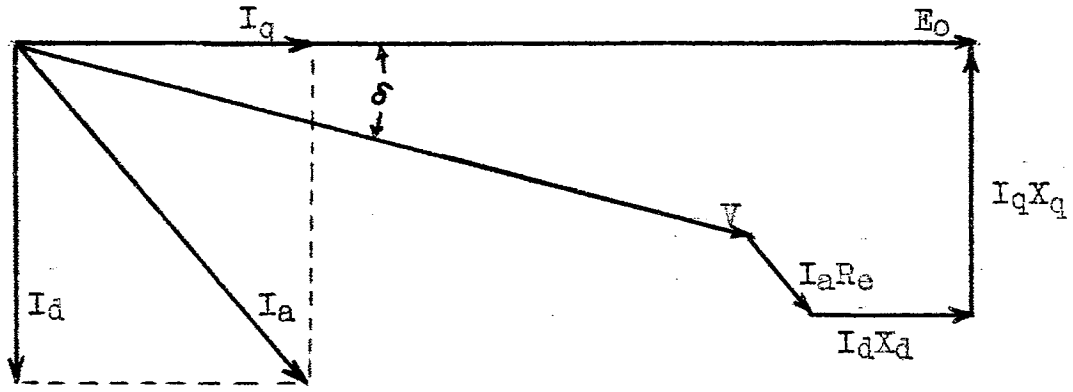

Figure I-1. Per phase vector diagram of a salient-pole machine.

X_q - Quadrature-axis reactance.

X_d - Direct-axis reactance.

ϕ - Total flux effective in developing E_o.

Making use of the double-reactance theory it may be shown that the power in the circuit, per phase, is

$$P = \frac{V^2\left[\frac{X_d - X_q}{2} \sin 2\delta - R_e\right] + VE_o\left[R_e \cos\delta - X_q \sin\delta\right]}{R_e^2 + X_d X_q}$$

Neglecting R_e as small in comparison with X_d and X_q,

$$P = \frac{VE_o \sin\delta}{X_d} + \frac{V^2(X_d - X_q)\sin 2\delta}{2 X_d X_q}$$

The first term of this expression constitutes the total power in the circuit for a cylindrical rotor machine. The second term is evidently present because of saliency and often is referred to as reluctance power.

The term is interesting. Notice the absence of E_o. Apparently no back e.m.f. is necessary. Even though E_o be of zero magnitude due to absence of field current, power is still available provided there is a difference in machine reactances along the direct and quadrature axes. One might conclude that such a machine is capable of delivering motor power without a rotor field. Such conclusions are erroneous and stem from the popular tendency to use electric circuits and circuit analysis to explain the behavior of machinery wherein magnetic circuit phenomena are much involved. The above mentioned tendency is

easily explained; it makes for simplicity.

Most practical applications of electric energy makes use of equipment having definitely defined electric circuits and definitely defined magnetic and/or electric fields. Rotating machinery in particular has a rather complicated system of magnetic circuits, combinations of which must occur in a precise manner if the machine is to perform with any predictable results. The electrical circuits of the machine, on the other hand, are easy enough to describe with equivalent terminals, junctions, e.m.f.'s and impedances. Furthermore, conventional instruments are available for making measurements of electric circuit parameters, and simple methods for the determination of magnetic circuit parameters are not available. It is no wonder that an attempt is always made to incorporate in a circuit diagram equivalent parameters which control the currents and voltages of the circuit in the same manner that the magnetic parameters on the physical machine control those quantities. These attempts have met with success in many applications. A complete analysis of motor power, however, requires a detailed investigation of the magnetic circuit and an understanding of the behavior of magnetic fields in iron circuits.

PART II

The Stator Field

The transfer of power across the air gap of the salient-pole synchronous motor is possible because of the interaction of two magnetic fields, both of which are rotating in the same direction and at the same speed. One of these fields originates in the stator and the other in the rotor. The interaction mentioned above is the tendency for the rotor field to "lock" in step with the stator field. The origin of the stator field will now be considered.

Take, for example, a single-phase, two-pole machine and refer to Figure I-2.

Let ϕ_a be the field flux caused by coil A alone, and assume that coil A draws from the line an exciting current such that $\phi_a = \phi_m \text{ Cos } \omega t$. Let coil B receive excitation from the same single-phase line, but by making use of some phase-shifting circuit allow the exciting current in coil B to lag that in coil A by ninety electrical degrees. If both coils provide the same magnetomotive force then ϕ_b will be given by the equation, $\phi_b = \phi_m \text{ Sin } \omega t$. Coil B is physically located ninety mechanical degrees around the periphery of the stator from coil A. With the coils simultaneously excited there exists two stator fluxes, one in the vertical axis and one in the horizontal axis, pulsating sinusoidally with time. A second fact which is very significant is that the time phase difference between the fluxes is ninety electrical degrees. Lines of magnetic flux actually exist only as a tool of the imagination in describing the force

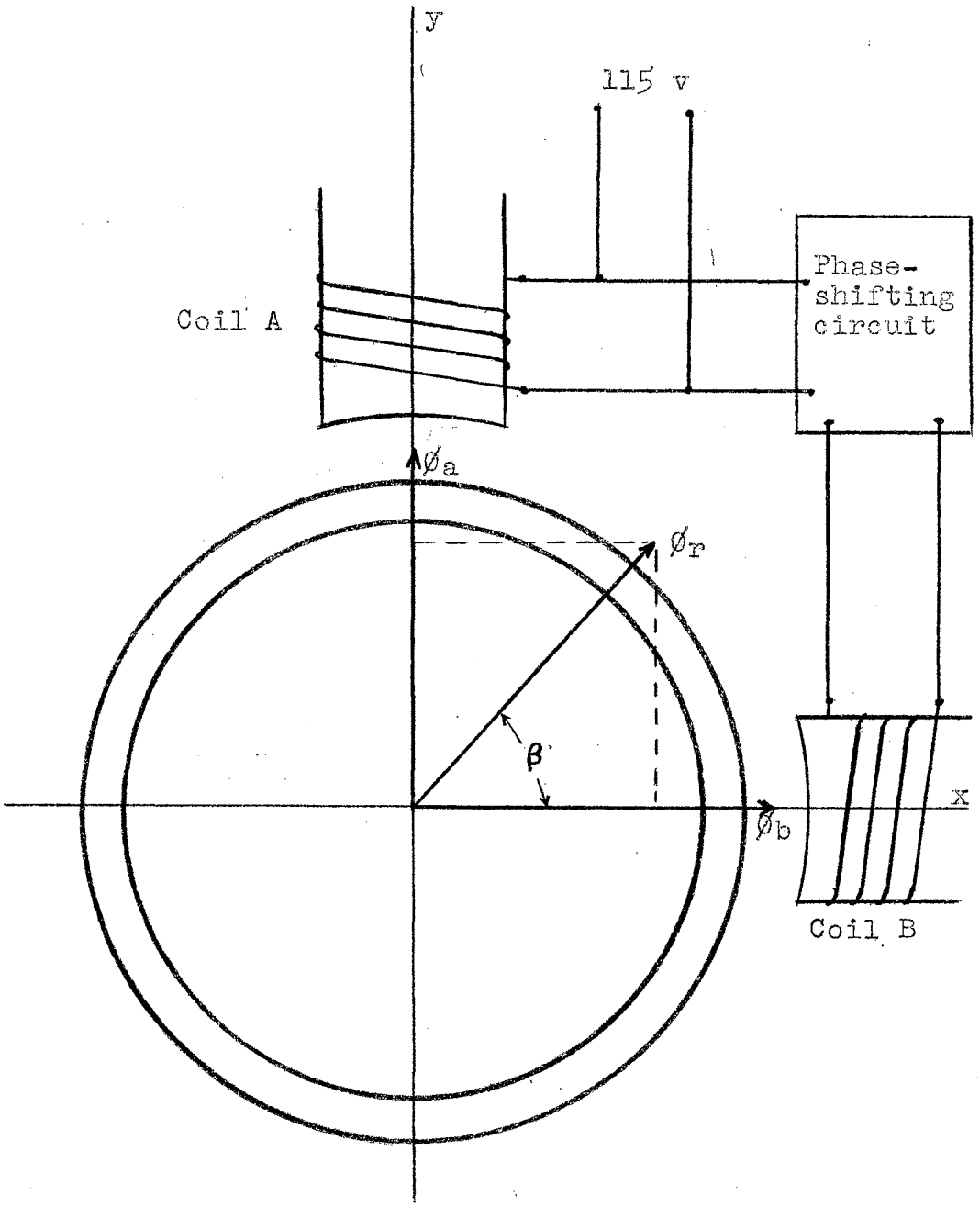

Figure I-2. Diagram showing position and magnitude of the resultant stator flux for one instant of time.

field of electro-magnetism. (According to one theory, which seems as good as any, even the force fields of permanently magnetized materials originate with electric motion within the atoms of the material). Thus the force fields originating in coils A and B cannot be considered separately, and it is the resultant flux with which one must deal in the analysis of the magnetic circuit.

This flux is readily found from

$$\phi_r = \phi_b + \phi_a$$

$$= \underline{i}\,\phi_m \operatorname{Sin} \omega t + \underline{j}\,\phi_m \operatorname{Cos} \omega t$$

The symbols $\underline{i}$ and $\underline{j}$ are introduced to indicate the space direction of the fluxes, $\underline{i}$ being assigned direction along the positive x-axis and $\underline{j}$ along the positive y-axis. ($\underline{j}$ is not to be confused with the conventional $\underline{J}$ of complex time varying quantities).

Let us determine the magnitude of ϕ_r as a function of time. Evidently

$$\text{Magnitude of } \phi_r = /\phi/ = \sqrt{\phi_m^2 \operatorname{Sin}^2 \omega t + \phi_m^2 \operatorname{Cos}^2 \omega t}$$

$$= \sqrt{\phi_m^2 (\operatorname{Sin}^2 \omega t + \operatorname{Cos}^2 \omega t)}$$

$$= \phi_m$$

The interesting result is that ϕ_r is constant with time and equal in magnitude to ϕ_m. The space location of ϕ_r is also of great importance. To this end let us determine the value of the angle β. Regardless of time the sine of β may always be determined from

$$\operatorname{Sin} \beta = \frac{\phi_m \operatorname{Cos} \omega t}{\phi_r}$$

or we may write

$$\beta = \text{Sin}^{-1} \frac{\phi_m \text{ Cos } \omega t}{\phi_r}$$

but

$$\phi_r = f(t) = \phi_m,$$

so

$$\beta = \text{Sin}^{-1} \frac{\phi_m \text{ Cos } \omega t}{\phi_m}$$

$$= \text{Sin}^{-1} \text{ Sin}(\omega t + 90)$$

$$= (\omega t + 90^\circ)$$

Now β is seen to be a function of time causing the resultant flux to rotate at the angular velocity of the line frequency. This is a very desirous effect, since it is this rotating flux which makes possible the motor action in the single-phase reluctance motor.

The phenomenon described above is frequently employed in the starting of small single-phase induction motors. These machines, small though they may be, are large by comparison with the one one-hundredth horsepower motor of our present consideration. Frequently, after starting, the quadrature field winding of the induction motor will be automatically removed by contactors operating from centrifugal force. The continuous duty rating of the phase-shifting circuit for the reluctance motor of this study, however, is sufficient to allow it to be permanently connected.

Part III

The Rotor Field

As mentioned in Part II of this chapter, motor action is dependent upon the inter-action of two fields. One of these fields, the driving field, originates in the stator. The other, the driven, must originate in the rotor. By this it is meant that the circulating charge responsible for the magnetic flux of the rotor is physically associated with the rotor itself. This concept is rather easily grasped when the induction motor is taken as an example. The revolving stator field develops an e.m.f. in the rotor winding. The circulating current of the rotor winding results in the rotor field which revolves with respect to the rotor. The rotor field is driven by the stator field at synchronous speed and motor action results. The significance of the example is that the driven field must be considered to be produced by currents which flow about the rotor, the driven member.

The reluctance motor has no rotor winding, or if it does have it serves only to furnish induction motor power during starting. Certainly at synchronous speed such a winding contributes no average motor torque. The origin of the rotor field is, of course, due to the ferromagnetic nature of the material from which the rotor is constructed. Since this plays such an important role in the functioning of the reluctance motor a qualitative explanation of the theory of magnetism will be

presented here.[2]

The smallest sub-division of magnetic matter, the atom with its nucleus and electrons, may be assumed as the origin of the magnetic flux line. (The flux line, as such, is non-existent but is a convenient tool of the imagination with which effects of the phenomenon may be described). The magnetic flux line possesses capabilities which can only be attributed to the energy of the moving electrons of the atom, and the source of this energy is no more readily explained than is the source of energy which causes the earth to move about the sun. Science has, on the other hand, made very powerful observations concerning the relationships existing between moving electric particles and resulting magnetic fields.

Refer to Figure I-3. Assume that the charge, q, is progressing along line ab at velocity $\vec{v}$. A magnetic field, $\vec{\phi}$, will be set up and described by the following equation:

$$\vec{\phi} = \frac{q}{r^2} (\vec{l}_r \times \vec{v}) \qquad (I\text{-}1)$$

where

$\vec{\phi}$ is the vector flux,

$\vec{l}_r$ is the unit radius vector,

$\vec{v}$ is the vector velocity.

The cross-product of the directional unit vector, $\vec{l}_r$, with $\vec{v}$ defines a flux vector into the plane of the picture at the point,

---

[2] The subject matter pertaining to the theory of magnetism is taken largely from the M.I.T. publications, Magnetic Circuits and Transformers, in which credit is given to R. M. Bozarth and his paper, "Present Status of Ferromagnetic Theory," A.I.E.E. Transactions, Vol. 54 (1935), p. 1251.

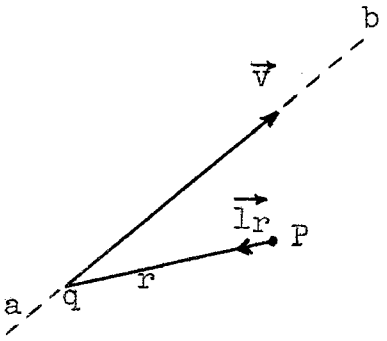

Figure I-3

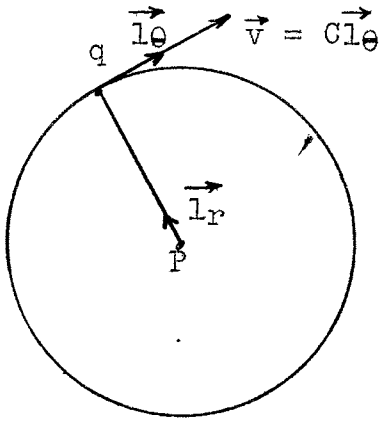

Figure I-4

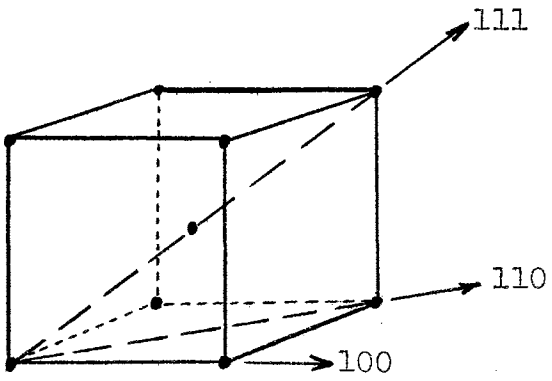

Figure I-5 Body-centered cubic lattice of iron crystal showing possible directions of magnetism. (From footnote reference 2.)

P. It is not conceivable that the charge, q, will move unless an electric field exists along the direction defined by the line ab. Now consider that at the atomic level of sub-division of matter an electric field exists in which a unit charge is forced along an orbit about the nucleus of the atom. As long as the velocity of the charge remains constant a magnetic flux of constant value will exist defined by a special case of equation (I-1). This is evident from a study of Figure I-4. The value of this flux is given by,

$$\vec{\phi} = \frac{q}{r^2} C(\vec{1}_r \times \vec{1}_\theta)$$

$\vec{1}_r \times \vec{1}_\theta = 1 \text{ Sin } 90^\circ = 1$, r is constant, and the magnetic flux vector, $\vec{\phi}$, can have only a constant magnitude with direction into the plane of the picture.

A single atom may have several orbits of the type described by Figure I-4, some with positive-spin and some with negative-spin electrons. Certain materials such as chromium, iron, cobalt and nickel have an excess of positive-spin electrons and, consequently, have a resultant magnetic moment of magnitude greater than zero at the atomic level.

A sub-division of matter known as the domain has a very sharp bearing on the magnetic properties of the material. In size the domain is somewhere between the atom and crystal. It is characterized by the fact that throughout the domain the material is completely magnetized at all times. The direction of magnetization may be changed from one to any of several other possible axes of magnetic moment, but such changes occur com-

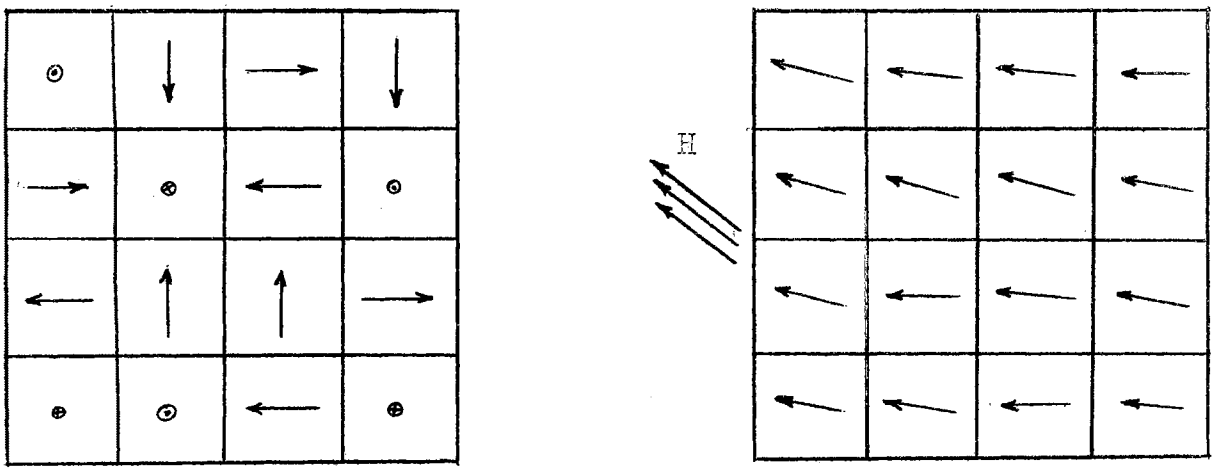

Figure I-6. a shows a crystal in unmagnetized state. b shows the same crystal under the influence of a relatively high external field, H. (From footnote reference 2)

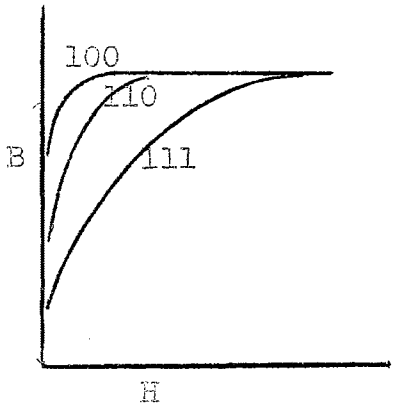

Figure I-7. Magnetization curves for an iron crystal in the directions 100, 110, and 111 (from footnote reference 2)

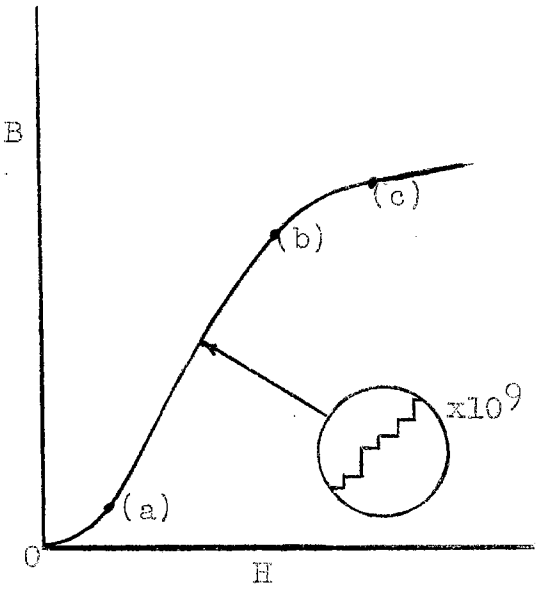

Figure I-8. The three regions of the magnetization curve: (0-a) boundary displacement, (a-b) sudden change in orientation, (b-c) slow change in orientation. (From footnote reference 2)

pletely and instantaneously. The arrangement of atoms in such a domain of the iron crystal is shown in Figure I-5. This is called a body-centered cubic lattice and the possible directions of magnetism are indicated by the arrows labeled 100, 110, and 111. The preferred direction of magnetization is along the 100 axis. The next least difficult direction is along the 110 axis, and the most difficult along the 111 axis.

An iron crystal may be thought of as consisting of a large number of domains each magnetized in the preferred direction but as many with a negative sense as with a positive sense. This situation is shown in Figure I-6 which represents a cross section of the crystal.

The mass of material as a whole is made up of many crystals. Iron, cobalt, and nickel have crystaline structures such that the magnetic moments of the individual crystals may be made to add, giving a net magnetic moment for the total mass.

Figure I-7 shows the relative ease with which the iron crystal may be magnetized along the three possible axes. Figure I-8 shows a typical magnetization curve for iron. The general shape of this curve is explained as follows. The section from 0 to (a) results from a growth of size of the domains.[3] The section from (a) to (b) results from the aligning of the magnetic moments of domains along an axis most nearly parallel to the applied field. It is noticed that this section of the curve is characterized by considerable increases in B for an incre-

---

[3] This phenomenon is not discussed in this work. The reader is referred to R. M. Bozarth, Op. cit., p. 1251.

ment of H. If the curve were magnified many times this portion would appear to change in steps. (See Figure I-8). This is due to the instantaneous switching of axes of magnetization within the domain. Some steps are higher than others because for some increments of H more domains yield to the external field than for other increments. The final section of the curve, (b) to (c), derives its shape from the gradual rotation of domains into the line of the impressed field. This is accomplished at considerable cost of energy, thus explaining the decrease of slope along this portion of the curve. When all domains have been rotated into position no further source of magnetism is available from the material and the sample is said to be saturated.

The entire discussion of magnetic theory as presented here is to substantiate the argument that the rotor of the reluctance motor produces its own field. Assume a hypothetical rotor of a material which will admit magnetic flux readily, but which has no such magnetic moment of its own as that just described. A substantial air-gap flux might exist produced by the stator winding. Now replace the above rotor with one of iron, a material with a local magnetomotive force at the atomic level. The air-gap may now be considered to have two fluxes; one of the same magnitude as the machine with the hypothetical rotor and one produced by the net magnetic moment of the iron rotor itself. The inter-action of these two fields results in motor action if the stator field is caused to rotate as described in Part II of this chapter. The amount of motor torque available depends upon the ability of the rotor to add to the air-gap flux. This

ability, of course, depends upon the material of which the rotor is constructed and upon the processing during manufacture.

CHAPTER II

Air-Gap Analysis of the Reluctance Motor

PART I

Introduction

Chapter III of this work presents a method of performance calculation making use of equations which are somewhat empirical in nature. The equations are, however, under the control of the design engineer to a certain extent. For instance, any change in processing of the steel used for rotor punchings which results in a more advantageous use of the natural magnetic moment of the metal would allow greater torque. The geometric construction of the several elements of the motor might be altered resulting in altogether different performance characteristics. These differences would be evidenced by changes of the equations in Chapter III. It is the purpose of the present chapter to develop a line of reasoning upon which interpretations of those equations may be based.

The reader is reminded that motor analysis, to be complete, must include an analysis of the behavior of the magnetic circuit. This is particularly true of the reluctance motor, a machine the very name of which attracts attention to its air-gap. The discussion which follows will develop the idea that a change in load results in a change of the reluctance of the magnetic circuit, and this in turn results in a change of input. Assume a single-phase, four-pole, reluctance motor to be operating lightly loaded. If simple measurements of input power, current, and line voltage were made, and if an equivalent series circuit were

calculated the circuit would be found to contain resistance and inductance in series. These parameters could not be identified as physical parameters of the stator alone even though the rotor turns at synchronous speed and no measurable quantity of current flows in the rotor. Now allow an increment of load to be added to the shaft. If the motor continues to carry the load at synchronous speed more energy must be extracted from the supply line. The only way this can be accomplished is by a variation of the equivalent connected impedance. The only control that the motor has over this is within the air-gap. Physically, an instantaneous but short-lived decrease of rotor speed causes a new set of conditions to exist between the rotor and stator fields. The adjustment must result in precisely the change of equivalent circuit necessary to draw from the line the increase in output power plus the increase of losses if any. The new equivalent impedance was brought about by a change of reluctance in the magnetic circuit, yet the change of equivalent impedance was not one of reactance alone. It is the complex manner in which the equivalent circuit of the reluctance motor changes under load that leads to the following rather unique analysis.

PART II

Energy Flow

Figure II-1 portrays the motor as a conservative system bounded by dashed lines. Energy, without regard to its form, flows into the system from the 115 volt line and flows from the system at the boundary representing the shaft and at other points to account for heat and friction losses. That part of the total which represents output plus friction loss must flow from the stator into the rotor, and in doing so must flow through an air volume. This is accomplished using as a vehicle the magnetic field. Since, for symmetrical construction, conditions are similar at each pole, for a four-pole motor one-fourth of the output plus friction loss flows into the rotor through a volume bounded by a-b-c-d in the plane of Figure II-1 and by the effective length of the rotor. The rate of flow of this energy depends upon the square of the flux density, the effective volume, and the speed of the machine. The energy density in a volume containing magnetic flux will now be determined.

The cube of Figure II-2 may be considered to have unit dimensions in the Rationalized MKS system. Allow a flux density, $\underline{B}$, to exist, and to explain its presence assume one turn of a conductor carrying enough current to maintain the flux in the volume. Since the volume is of unit length the magnetic field intensity, $\underline{H}$, is given by:

$$H = NI$$

If the current varies this may be written

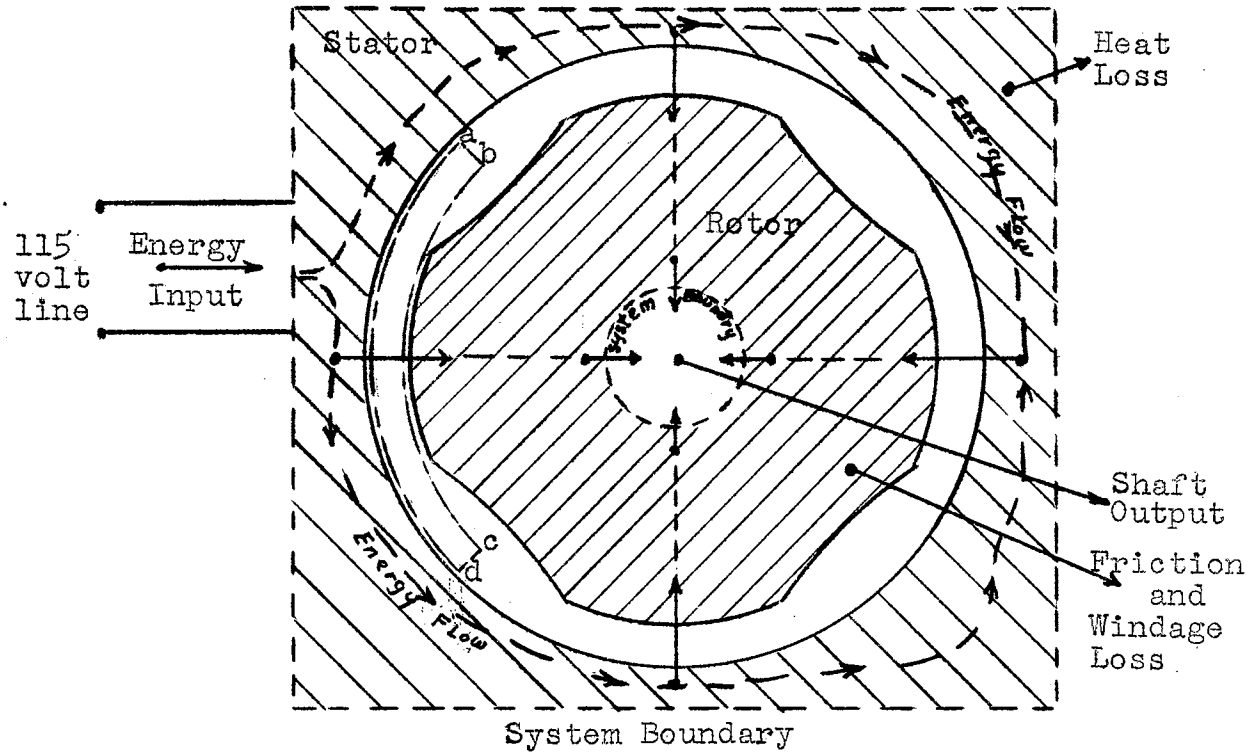

Figure II-1. Motor represented as a conservative energy system

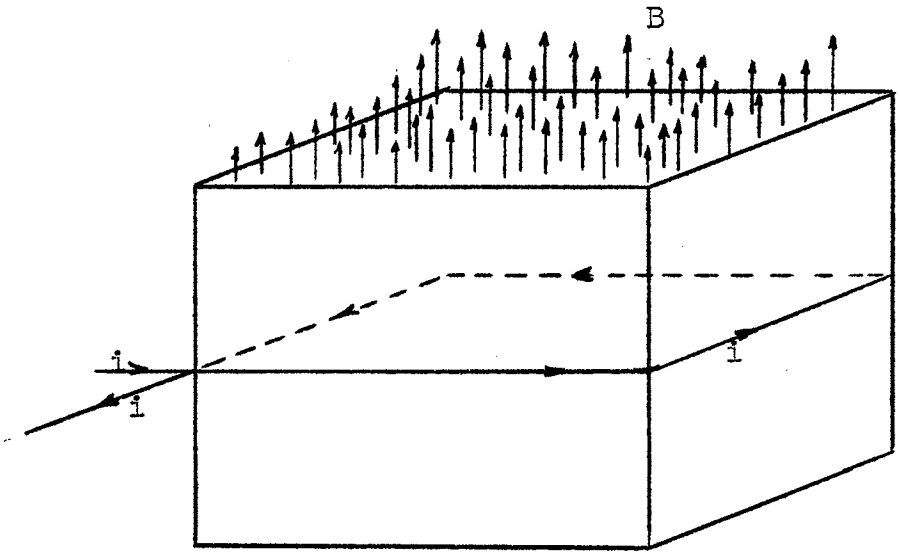

Figure II-2. Unit volume containing magnetic flux

$$\mathcal{F} = Ni \qquad \text{(II-1)}$$

When the current is established from zero the equation for dynamic equilibrium is

$$e = Ri + N\frac{d\phi}{dt}$$

$$= Ri + NA\frac{dB}{dt} \qquad \text{(II-2)}$$

where A is the cross-sectional area normal to the flux, unity in this case.

The energy input to the magnetic field while establishing the current, I, is

$$W' = \int_0^I N\frac{dB}{dt}\, i\, dt \qquad \text{(II-3)}$$

Substituting for i from equation II-1 into II-3 the following is obtained:

$$W' = \int_{0\ at\ i=0}^{B\ at\ i=I} \frac{N}{N}\mathcal{F}\, dB = \frac{1}{\mu}\int_0^B B\, dB \qquad \text{(II-4)}$$

where μ is the permeability of air and relates B and H as $B = \mu H$. Integrating equation II-4 provides an equation for the energy stored in a unit volume of air containing a flux density of B Webbers per square meter. The result is

$$W' = \frac{B^2}{2\mu} \quad joules \qquad \text{(II-5)}$$

Equation II-5 may be extended in scope by considering it as an expression of energy density. The total energy in any air volume is therefore,

$$W = \int_v \frac{B^2}{2\mu}\, dv \qquad \text{(II-6)}$$

The use of the hypothetical magnetomotive force in Figure II-2 was simply a means to an end. The final result (and the desired result) is that where a magnetic field exists, regardless of how it came to be there, there is a quantity of stored energy which may be calculated from equation II-6.

The application of equation II-6 to a practical motor problem is considerably more involved than its derivation. It would be very impracticable to try to express $\underline{B}$ as a mathematical function of the volume of the air-gap. But the equation does serve to show that the size and shape of the air-gap in conjunction with the flux density is a measure of the energy storage, and a method of calculating energy flow from energy storage will now be developed.

Let $\underline{P}'$ be the total mechanical power of the rotor consisting of windage and friction loss plus the shaft load. The machine operates at a constant speed and the former may be considered as additional shaft load. The rate of energy flow into the rotor through the air-gap is $\underline{P}'$ joules per second. Figure II-3 represents one position of the rotor while driving the load, $\underline{P}'$. For simplicity the discussion will be centered around only a single pole, and $\frac{P'}{4}$ joules per second will be the rate of energy flowing into the rotor in the medium of the magnetic field at that pole. The area a-b-c-d has but one requirement as to dimensions; the length, b-c, must be equal to the pole pitch. The flux passing through the volume created by this area and the effective length of the rotor is shown as two components. The solid lines represent the stator field. This is the constant,

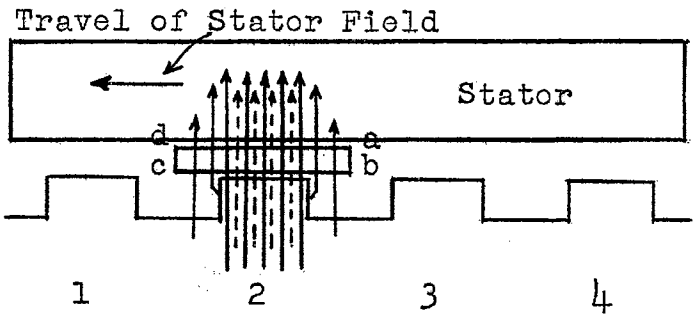

Figure II-3

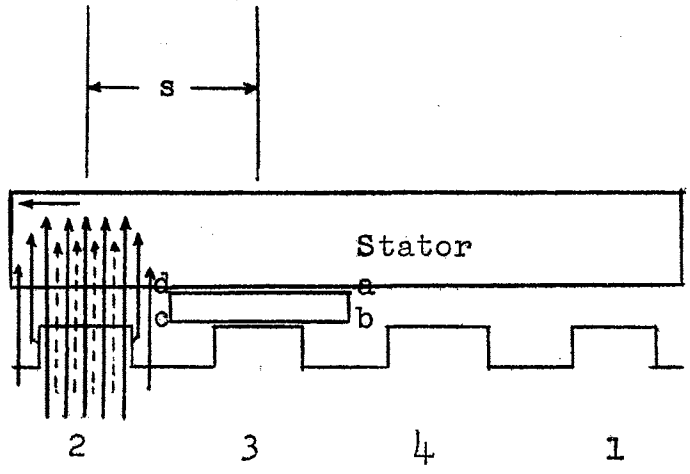

Figure II-4

rotating field as developed in Chapter I. The dotted lines represent the field produced by the rotor. The meshing of the fields allows motor action, and it is the density of the total flux which determines the energy storage. Figure II-4 shows the same set of fields a short while later assuming a point on the rotor to have moved through one pole pitch. In this picture the volume, (a-b)(b-c) x effective rotor length, is shown to be void of flux eminating from the number-2 pole. The energy present in the volume as shown in Figure II-3 has diminished to zero as shown in Figure II-4. (There will be flux present in the volume because of the number-3 pole, but this development is on a per-pole basis). The average rate of decrease of energy in the volume is the rate at which energy flows into the rotor through the field established by the number-2 pole. This may be expressed mathematically by the following equation:

$$\frac{P'}{4} = \frac{W}{\Delta t}$$

where W is the energy stored in the volume and Δt is the time for 1/4 revolution. When the machine operates from a 60-cycle line the rotor speed is 1800 rpm and Δt is easily found to be 1/120 second. The expression for total mechanical power becomes

$$P' = 480\ W \quad \text{watts} \qquad \text{(II-7)}$$

where

$$W = \int_v \frac{B^2}{2\mu} dv \qquad \text{(II-6)}$$

No mention has been made of the distribution of flux throughout the volumes shown in Figures II-3 and II-4. It was

not necessary in the derivation of equation II-7. For the evaluation of $\underline{W}$, however, employing equation II-6, the distribution of $\underline{B}$ as a point function throughout the volume must be known.

As previously suggested such a function is rather difficult to obtain. The most logical approach to the problem is a graphical solution entailing the mapping of the flux pattern within the air-gap. It is not the purpose of this thesis to do that, but a qualitative discussion will bring out the importance of the concept.

Suppose that an increment of shaft load be added to the machine as represented in Figure II-3. Obviously something in the picture must change. The value of the integral in equation II-6 must increase to supply the additional load. The source of energy (the 115 volt line) must be informed electrically (or magnetically, or both) that additional power is to be furnished. Personification is used here to emphasize the importance of the use of variable-reluctance rotor construction. The equivalent impedance of the motor takes on new values, but not until some change in Figure II-3 is accomplished. This change is effected by a momentary deceleration of the rotor without a corresponding momentary acceleration. This results in a shift of rotor position with respect to stator field. Because of the saliency of the rotor punchings a change of reluctance is inserted in the magnetic circuit and a redistribution of flux throughout the volume results. The flux density may be decreased at some points within the volume, but the increase at other points suffices to

overcome this. If the machine is to carry the additional load there must be an increment in the value given by equation II-6.

Observe that if the rotor were of cylindrical construction the shift of position with respect to the stator field (assuming that it was rotating in the first place) would in no manner effect the looking-in impedance of the motor and, therefore, could not accommodate the increment in load. This idea may be extended to include the case where the increment is the first increase of load attempted.

CHAPTER III

Analytical Analysis of Performance

PART I

Introduction

Small motor performance is most often determined by the trial and error method. In practice this method makes use of a vast reservoir of statistics and data from previously manufactured machines. With this information at hand, a trial motor is designed and actually constructed. The first machine is not necessarily expected to meet performance requirements, but it is an existing device which may be tested and studied. From it a second trial machine may be designed and as likely as not the latter motor will perform within specifications. This procedure may appear costly but where a large number of miniature motors are to be made from a design, once it has been found, the cost of test models is a very small fraction of the total production cost. Furthermore, test data from trial motors becomes a worthwhile addition to the statistical reservoir.

There really is no good substitute for the above procedure in the manufacture of motors with output of from $\frac{1}{100}$ to $\frac{1}{8}$ horsepower. Such motors (particularly those in the size range with which this paper deals), consume in losses a large percentage of the total input power. For instance, the constant part of the losses of the $\frac{1}{100}$ horsepower motor used in this sutdy is above 20 watts. Compared with 7.46 watts this is above 260% of the rated output. It is entirely possible that a minute change in bearing location on a future model would change this loss by 30

to 40%, either up or down. Such an item has far less effect in the design of larger machines where the windage and bearing friction represents only a few percent of the total input. So, for large motors, performance may be fairly accurately predicted before the plans leave the designing board, but for the miniature machines a complete prediction of performance is most unlikely.

This chapter will present a method of analysis to be used in the study of the test model. The method assumes curves of input current, input power, power factor, and losses versus output power to be the most important performance considerations.

PART II

The Geometric Pattern of Current Vectors as Found from Test Data

Circle or semi-circular diagrams have long been useful tools in the derivation of and interpretation of equivalent circuits for electrical machinery. From these diagrams one may see how the natural or equivalent parameters of the machine vary with load changes. In some cases complete performance predictions are based upon the diagram. With the importance of this precedent in mind the loci of current vectors for the motor of this study will be found.

Figure III-1 is a record of performance characteristics from tests performed on the motor by the Robins-Meyers Company. Values for Table II were taken from the curves. The table is

Table II

	Current	Power Factor	Angle	Watts In	Watts Out	Percent Efficiency
1	.386	.643	50°	29.0	0	0
2	.395	.669	48°	30.5	2.0	6.6
3	.406	.694	46°	32.5	4.6	14.2
4	.419	.710	44.75°	34.5	6.7	20.0
5	.428	.719	44°	35.4	7.5	21.2
6	.445	.731	43°	37.0	9.0	24.7
7	.460	.739	42.4°	38.5	10.1	26.5
8	.481	.731	43°	39.7	11.0	28.0
9	.496	.719	44°	41.0	11.7	28.6
10	.504	.710	44.75°	41.5	12.0	29.0

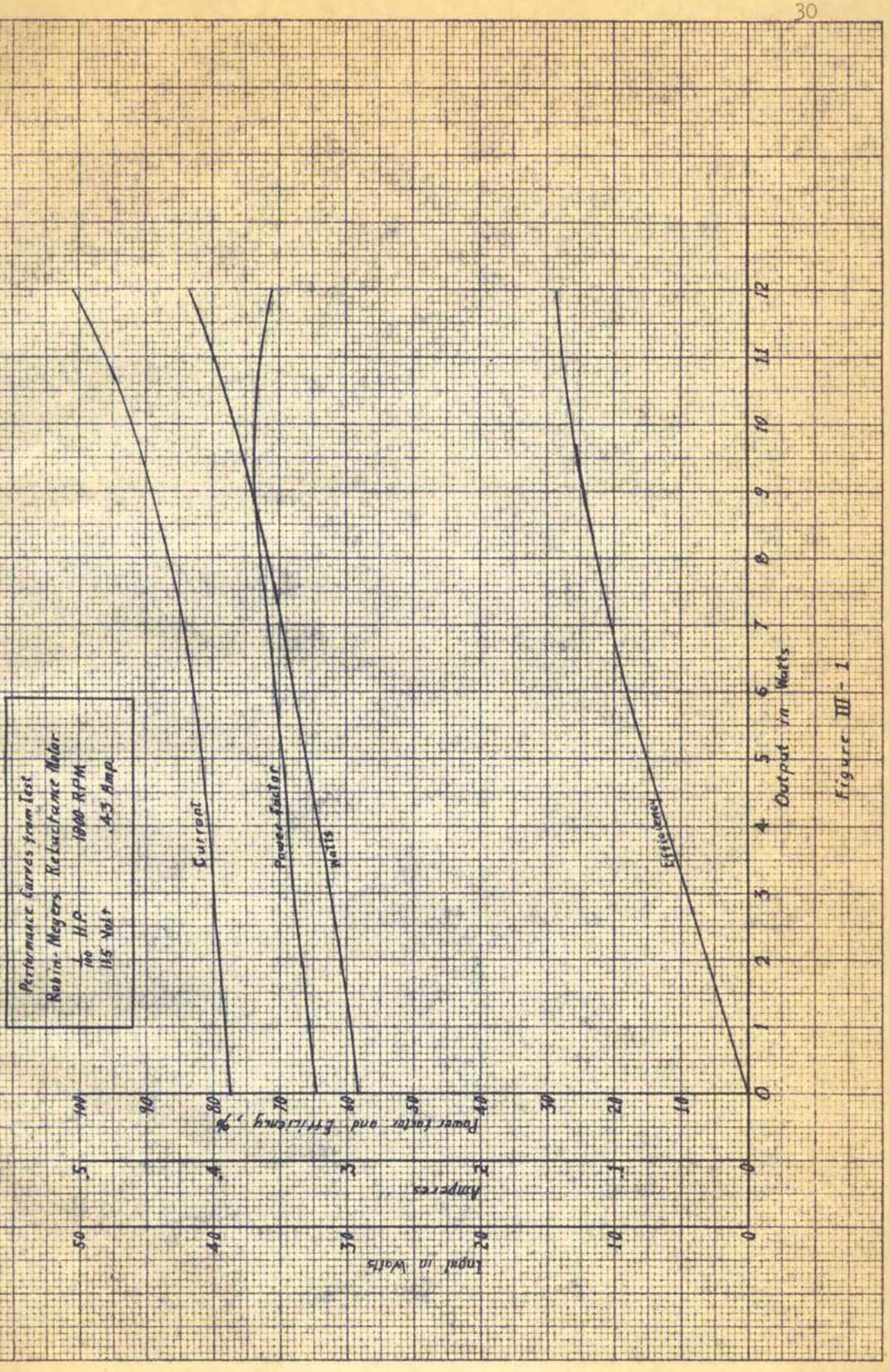
Performance Curves from Test
Robin-Meyers Reluctance Motor
1/6 H.P. 1800 RPM
115 Volt .43 Amp
Current
Power Factor
Watts
Efficiency
Output in Watts
Power factor and Efficiency, %
Amperes
Input in Watts

Figure III - 1

self-explanatory.

Figure III-2 shows the polar plot of the currents listed in Table II. The loci of current vectors from no-load to full-load is shown by the solid line. It may be observed from the plot that the points seem to lie on an elliptical path. It seems logical, then, to determine the equation for the ellipse which will most nearly plot the current loci. Toward this end the dotted remainder of the ellipse is added by trial and error, and the major and minor axes of the ellipse are located. Refer again to Figure III-2. If the origin of rectangular coordinates were at the intersection of these axes the equation of the figure would be:

$$\frac{x^2}{a^2} + \frac{y^2}{b^2} = 1 \qquad \text{(III-1)}$$

If $\underline{a}$ and $\underline{b}$ are measured to the current scale used for the original plotting, equation (III-1) becomes:

$$\frac{x^2}{.058^2} + \frac{y^2}{.082^2} = 1 \qquad \text{(III-2)}$$

or

$$2x^2 + y^2 = .00672 \qquad \text{(III-2)}$$

Before the curve of equation (III-2) can be useful its origin of coordinates must be translated to the position of the origin of current vectors shown in Figure III-2. In the rectangular system it is evident that any point, such as $\underline{P}$, on the curve is equally well described as P(x,y) or P(X-h, Y-k). Making use of the latter coordinates, equation (III-2) becomes:

$$2(X-h)^2 + (Y-k)^2 = .00672 \qquad \text{(III-3)}$$

To the current scale $\underline{h}$ and $\underline{k}$ are respectively .350 and .275.

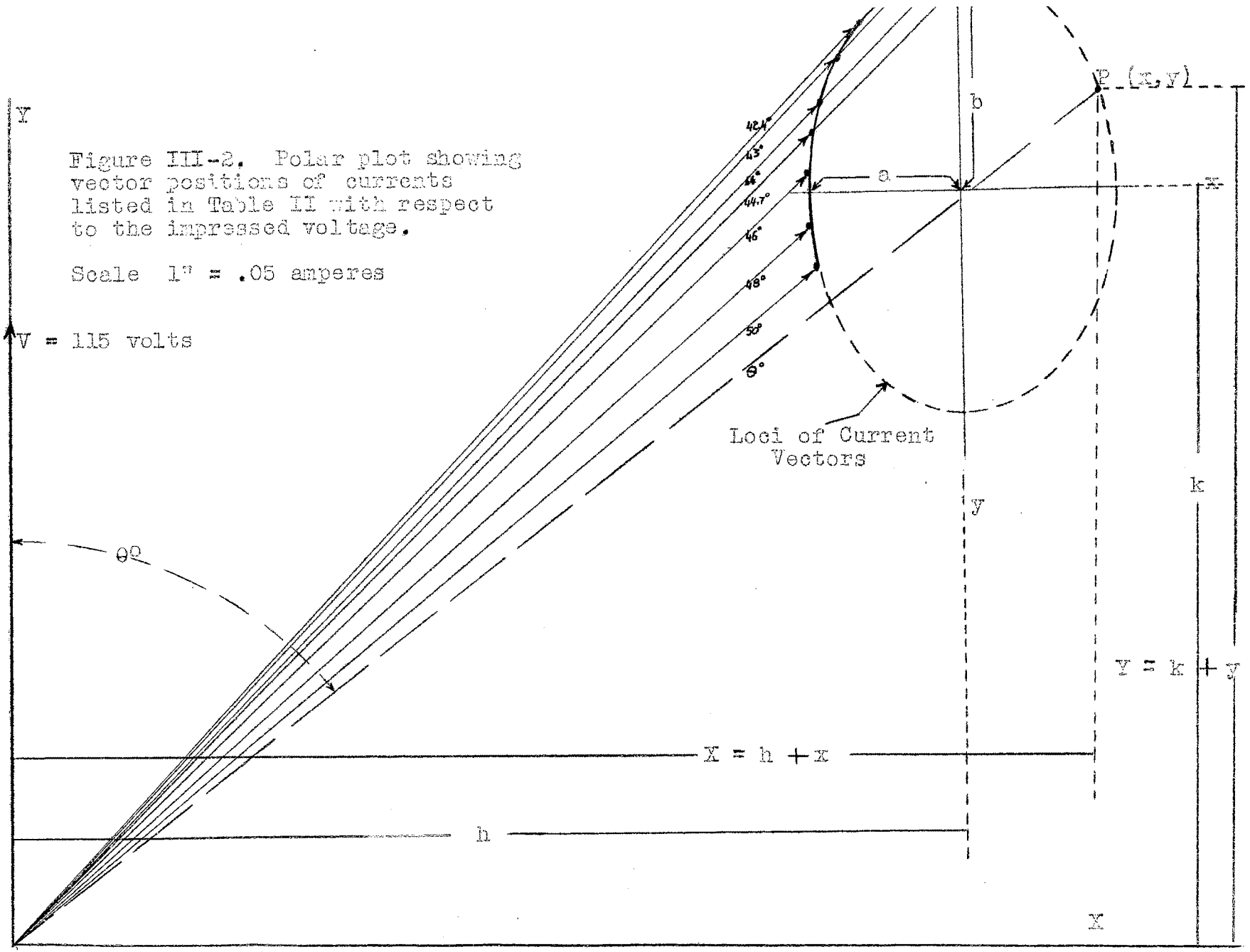

Figure III-2. Polar plot showing vector positions of currents listed in Table II with respect to the impressed voltage.

Scale 1" = .05 amperes

Making these substitutions, equation (III-3) becomes:

$$2(X - .35)^2 + (Y - .275)^2 = .00672.$$

Expanded and reduced,

$$2X^2 - 1.4X + Y^2 - .55Y + .314 = 0 \qquad \text{(III-4)}$$

Finally, this equation will be expressed in polar coordinates. Let $\underline{\theta}$ be the angle by which the current, $\underline{I}$, lags the voltage and let the voltage reference be taken along the Y-axis. Then the values of the $\underline{X}$ and $\underline{Y}$ coordinates of any point may be expressed as $\underline{I \sin \theta}$ and $\underline{I \cos \theta}$ respectively where $\underline{I}$ is the length of the current vector to the point in question. Making the appropriate substitutions, equation (III-4) becomes:

$$2(I^2 \sin^2 \theta) - 1.4(I \sin \theta) + I^2 \cos^2 \theta - .55(I \cos \theta) + .314 = 0 \qquad \text{(III-5)}$$

Thus, for various loads, the end points of the vectors representing the input current to the reluctance motor under consideration moves along a sector of an ellipse. It is not suggested that the current vector plot of all reluctance motors will follow an elliptical pattern. It is merely recognized that this is the case for the type under present consideration.

PART III

Calculation of Losses

A careful examination of test data reveals a peculiar variation of losses with load. From no-load to about 5 watts output there is a gradual decrease in total losses. From this load value to 160% load there is a gradual increase. Total line current increases with each increment of load, so the heating loss due to $I^2R_{(ohmic)}$ increases continuously with load. The machine operates at constant speed with the result that windage and bearing friction losses are constant throughout the operating range. The logical deduction from the foregoing is that there is an actual decrease in iron losses with load increases between no load and about 3/4 full load.

Fundamentally, the rate of energy dissipation due to changing fluxes in a given volume of iron may be determined from[1]

$$P_{(h + e)} = K_h f B_m^{1.6} + K_e f^2 B_m^2 \qquad \text{(III-6)}$$

where

$P_{(h + e)}$ = Power loss due to the hysteresis phenomenon + eddy-current power loss.

K_h = Hysteresis constant.

f = Speed or frequency of reversal.

K_e = Eddy-current constant.

B_m = Maximum flux density.

Equation III-6 applied to the single phase reluctance motor

---

[1] C. W. Ricker and Carlton E. Tucker, Electrical Engineering Laboratory Experiments, p. 221.

would calculate iron loss only in the stator of the machine. The rotor runs synchronously with the field and the frequency of flux reversal in the rotor is, therefore, zero. When load is applied to the motor the rotor position changes, increasing the air-gap. Introduction of greater reluctance in the magnetic circuit limits the flux, thereby reducing the iron loss. This is accompanied by a reduction in magnetizing current. Reference to Figure III-2 shows that from no-load up to the load corresponding to $\theta = 46^{\circ}$ the quadrature component of current actually decreases even though the energy component increases. Additional load beyond this point shows an increase of magnetizing current which is evidently accompanied by an increase of flux and core loss.

Since the ultimate interest is in characteristics of performance versus output, let it be determined how the total losses of the machine vary with load. For this purpose consider that at any load the total machine losses may be expressed by

$$P_t = P_v + P_c \qquad \text{(III-7)}$$

where

P_t = Total loss.

P_v = Total variable losses (i.e. core loss + $I^2R_{(ohmic)}$).

P_c = Constant loss.

If $\underline{P}_t$ now be evaluated for a large number of output points taking increments sufficiently small a derivative curve, $\frac{\Delta P_v}{\Delta P_o}$ versus $\underline{P}_o$, may be determined where $\underline{P}_o$ represents output power. To illustrate, $\frac{\Delta P_v}{\Delta P_o}$ will be evaluated for $P_o = 2.5$ watts. In general

TABLE III

Input	P_o, Output	Losses	$P_{(n+1/4)} - P_{(n-1/4)}$	$\frac{\Delta P_v}{\Delta P_o}$
29.10	.25	28.85		
	.50		-.15	-.30
29.45	.75	28.70		
	1.00		-.13	-.26
29.82	1.25	28.57		
	1.50		-.12	-.24
30.20	1.75	28.45		
	2.00		-.20	-.40
30.50	2.25	28.25		
	2.50		-.10	-.20
30.90	2.75	28.15		
	3.00		-.10	-.20
31.30	3.25	28.05		
	3.50		-.05	-.10
31.75	3.75	28.00		
	4.00		-.07	-.14
32.18	4.25	27.93		
	4.50		-.08	-.16
32.60	4.75	27.85		
	5.00		-.05	-.10
33.05	5.25	27.80		
	5.50		.05	.10
33.60	5.75	27.85		
	6.00		.00	.00
34.10	6.25	27.85		
	6.50		.00	.00
34.60	6.75	27.85		
	7.00		.00	.00
35.10	7.25	27.85		
	7.50		.05	.10
35.65	7.75	27.90		
	8.00		.10	.20
36.25	8.25	28.00		
	8.50		.10	.20
36.85	8.75	28.10		
	9.00		.15	.30
37.50	9.25	28.25		
	9.50		.00	.00
38.00	9.75	28.25		
	10.00		.00	.00
38.50	10.25	28.25		
	10.50		.25	.50
39.25	10.75	28.50		
	11.00		.25	.50
40.00	11.25	28.75		
	11.50		.50	1.00
41.00	11.75	29.25		

$$\Delta P_{v(n)} = P_{t(n+\frac{1}{4})} - P_{t(n-\frac{1}{4})} \qquad \text{(III-8)}$$

$$= (P_v + P_c)_{(n+\frac{1}{4})} - (P_v + P_c)_{(n-\frac{1}{4})}$$

$$= P_{v(n+\frac{1}{4})} - P_{v(n-\frac{1}{4})}$$

$$\Delta P_o = \text{The increment} = P_{o(n+\frac{1}{4})} - P_{o(n-\frac{1}{4})} \qquad \text{(III-9)}$$

where n identifies the value of P_c for which $\frac{\Delta P_v}{\Delta P_o}$ is to be found. (Refer to Figure III-1). Let

$$n = 2.5$$

$$n+\tfrac{1}{4} = 2.75$$

$$n-\tfrac{1}{4} = 2.25$$

For n = 2.5

$$P_t(2.25) = 30.5 - 2.25 = 28.25 = (P_v + P_c)_{2.25} \qquad \text{(III-7)}$$

$$P_t(2.75) = 30.9 - 2.75 = 28.15 = (P_v + P_c)_{2.75}$$

$$\Delta P_v(2.5) = P_t(2.75) - P_t(2.25) = -.1 \text{ watt} \qquad \text{(III-8)}$$

This quantity is obviously a differential of the variable losses.

$$\Delta P_o = P_{o(n+\frac{1}{4})} - P_{o(n-\frac{1}{4})} = 2.75 - 2.25 = .5 \text{ watt} \qquad \text{(III-9)}$$

$$\frac{\Delta P_v}{\Delta P_o} = -.2 \text{ for } P_o = 2.5 \text{ watts}$$

Table III lists the results of the above calculation for a number of points from no-load to 160% load. The results listed in this table have been plotted as the solid curve on Figure III-3. (Explanation of the dotted line will be presented later). The sole purpose in plotting $\frac{\Delta P_v}{\Delta P_o}$ versus P_o is to determine from the plot an expression for P_v versus P_o. The $\frac{\Delta P_v}{\Delta P_o}$ curve has the general appearance of an exponential. In order to investigate this possibility the following equation may be assumed.

$$\frac{\Delta P_v}{\Delta P_o} = A + B\epsilon^{KP_o}$$

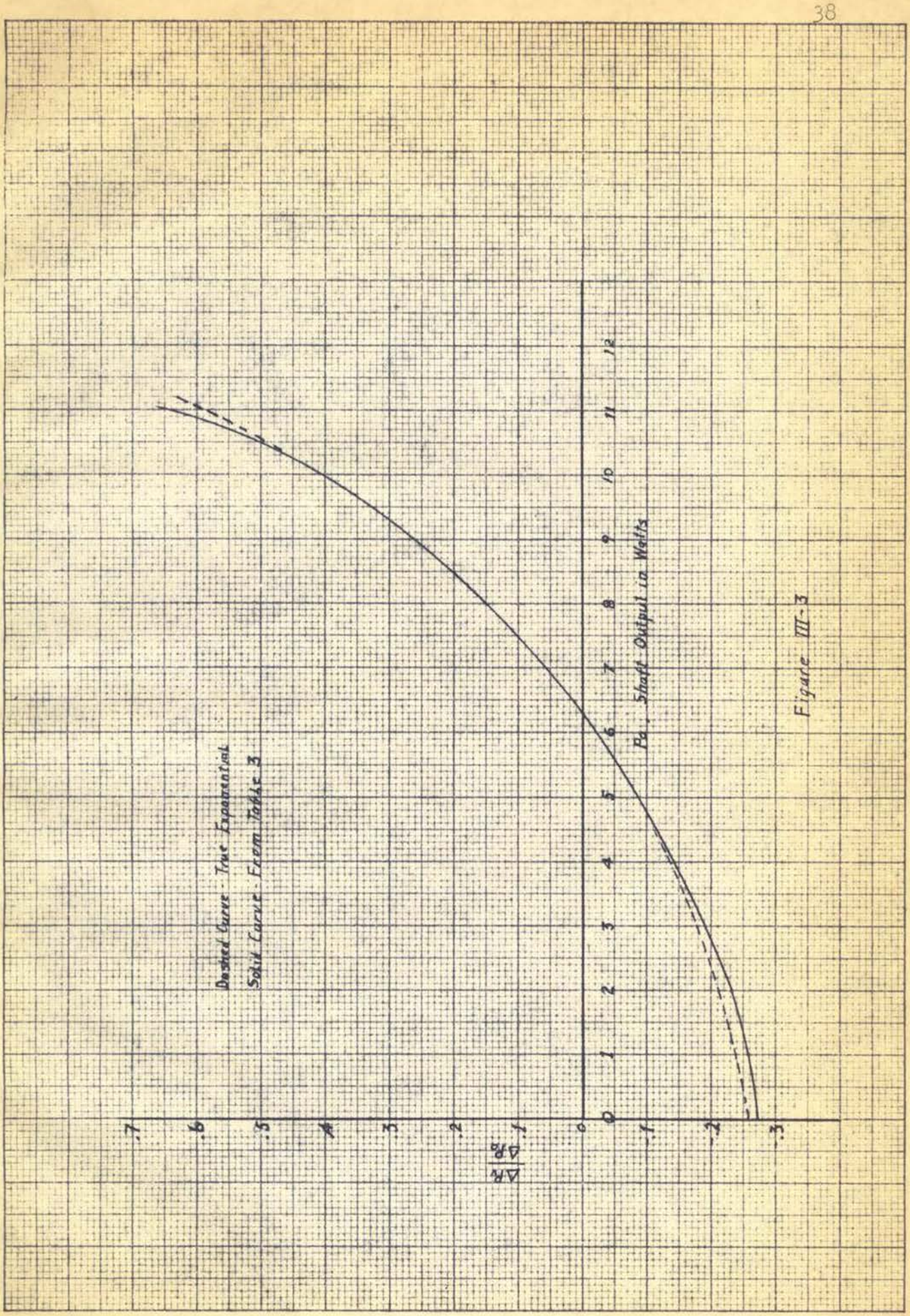
Dashed Curve - True Exponential
Solid Curve - From Table 3
$\frac{\Delta R}{R_0}$
P_d - Shaft Output in Watts
.7
.6
.5
.4
.3
.2
.1
0
-.1
-.2
-.3
0
1
2
3
4
5
6
7
8
9
10
11
12

Figure III-3

B, the multiplier[2] of the exponential, is .1. A may be evaluated from Figure III-3. When $P_o = 0$, $\frac{\Delta P_v}{\Delta P_o} = -.27$ and equation III-10 becomes

$$-.27 = A + .1$$

$$A = -.37$$

In order to evaluate K a plot of the exponential part of equation III-10 has been made in Figure III-4. For this plotting equation III-9 may be rearranged as

$$B\epsilon^{KP_o} = \frac{\Delta P_v}{\Delta P_o} + .37 \qquad \text{(III-11)}$$

and values for $\frac{\Delta P_v}{\Delta P_o}$ may be taken from the solid curve of Figure III-3. The straight line which results as an average of the plotting of equation III-10 now provides the constant, K, of the exponent. Its evaluation follows:

At $P_o = 6$ watts, $B\epsilon^{KP_o} = .34$ from Figure III-4.

$$B\epsilon^{KP_o} = .34$$

$$.1\epsilon^{K6} = .34$$

$$\epsilon^{K6} = 3.4$$

$$K = \frac{\text{Ln } 3.4}{6} = \frac{1.222}{6} = .203$$

With all terms thus evaluated the equation for the ratio curve, $\frac{\Delta P_v}{\Delta P_o}$ versus P_o, may now be written

$$\frac{\Delta P_v}{\Delta P_o} = -.37 + .1\epsilon^{.203P_o} \qquad \text{(III-12)}$$

A plotting of this equation reveals that if the constant, A, is adjusted to -.36 the curve will more nearly duplicate all points on the true curve as taken from Table III. Finally, then,

---

2 10^{-1} rather than some other power of 10 was chosen because, by observation, the exponential part of $\frac{\Delta P_v}{\Delta P_o}$ varies between .1 and 1.0.

Semi-Logarithmic Plot of the Exponential Part of Equation II-9

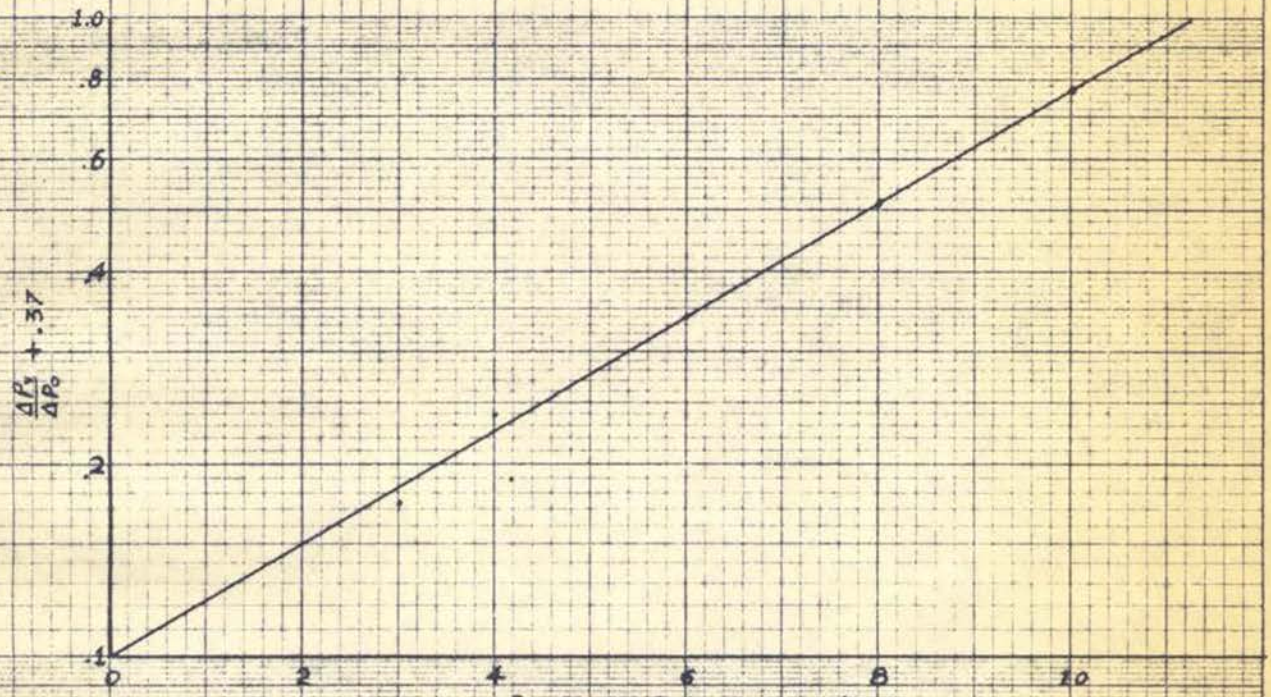

Figure III-4

the dashed-line curve of Figure III-3 is the graph of the equation,

$$\frac{\Delta P_v}{\Delta P_o} = -.36 + .1\epsilon^{.203 P_o} \qquad \text{(III-13)}$$

The use of equation III-13 will now be explained. The equation was derived on the assumption that $\frac{\Delta P_v}{\Delta P_o}$ is continuous (at least throughout the range with which we are concerned) with P_o. Therefore, the limiting value of the fraction, $\frac{\Delta P_v}{\Delta P_o}$, may be substituted and the equation becomes

$$\frac{dP_v}{dP_o} = -.36 + .1\epsilon^{.203\ P_o} \qquad \text{(III-14)}$$

The solution of the above is evident.

$$P_v = -.36\int dP_o + .1\int \epsilon^{.203\ P_o}\, dP_o$$

$$= -.36\ P_o + .493\epsilon^{.203\ P_o} + C \qquad \text{(III-15)}$$

Substituting equation III-15 into equation III-7 the expression for total losses becomes

$$P_t = -.36\ P_o + .493\epsilon^{.203\ P_o} + C + P_c$$

$$= -.36\ P_o + .493\epsilon^{.203\ P_o} + P_c' \qquad \text{(III-16)}$$

The term P_c' may be evaluated most readily from the knowledge that total losses are 29 watts at zero output. Under these conditions

$$P_t = 29 = .493 + P_c'$$

$$P_c' = 28.507 \text{ watts}$$

P_c' is not to be confused with the windage and friction loss alone. P_c' includes the constant of integration from the expression for copper and iron losses. Recall that these losses actually decrease from some initial value until a load of about 5 watts is reached. Figure III-5 clarifies these ideas.

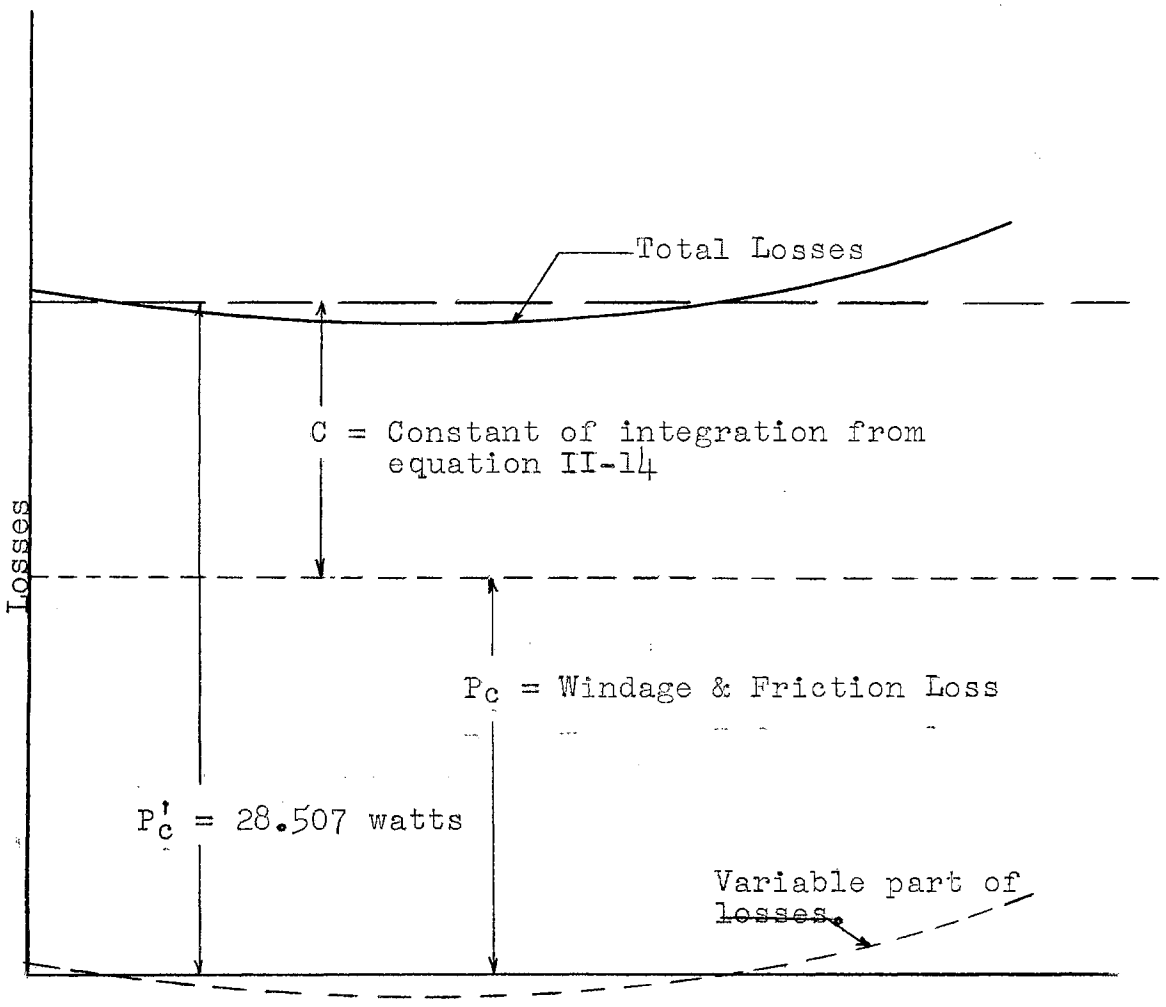
Total Losses
C = Constant of integration from equation II-14
Losses
P_c = Windage & Friction Loss
P_c' = 28.507 watts
Variable part of losses

Figure III-5

PART IV

Calculation of Performance

Equations III-5 and III-16 provide all the information necessary for a complete calculation of performance of the reluctance motor under consideration. This information is most readily available if the equations are expressed in graphical form. Let equation III-5 be repeated here.

$$2(I^2\sin^2\theta) - 1.4(I \sin\theta) + I^2\cos^2\theta - .55(I \cos\theta) + .314 = 0 \qquad \text{(III-5)}$$

The equation may also be written as

$$I^2 + I^2\sin^2\theta - 1.4(I \sin\theta) - .55\ I \cos\theta + .314 = 0$$

Values of $\underline{I}$ and of input corresponding to values of $\underline{\theta}$ are calculated in Tables IV and V. The information contained in Table IV is more useful when presented in graphic form. Refer, then, to Figure III-6. For any desired value of input, the current may be found and the power factor angle measured. The procedure is as follows. Enter the power axis with the desired input value converted to unit measure. Locate the current corresponding to this level on a portion of the curve in the stability range. The value of this current may be scaled on a straight line connecting the point with the origin. The power-factor angle is tan-1 Reactive Power/Power.

To find the input corresponding to any desired output value refer to Figure III-7. The loss versus output curve is determined from equation III-16. Computations for this curve are listed in Table VI. The input curve is plotted by adding the output to the loss curve.

The motor performance as calculated by the method of this chapter is seen to agree remarkably well with the laboratory test data plotted in Figure III-1.

Table IV

θ	$\sin\theta$	$\sin^2\theta$	$\cos\theta$	$1.4\sin\theta$	$.55\cos\theta$	Quadratic in I	Root 1 Root 2 Currents		Input IV $\cos\theta$	
42	.669	.448	.7431	.9370	.408	$1.448I^2-1.345I$ .314	Imaginary		--	--
44	.695	.482	.7193	.9710	.3955	$1.482I^2-1.366I$ .314	.428	.493	35.4	40.7
46	.720	.518	.6950	1.010	.3820	$1.518I^2-1.392I$ .314	.405	.510	32.4	40.8
48	.743	.552	.670	1.04	.368	$1.552I^2-1.408I$ .314	.395	.512	30.2	39.5
50	.766	.585	.643	1.07	.354	$1.585I^2-1.424I$ .314	.388	.511	28.7	37.8
52	.788	.621	.616	1.102	.339	$1.621I^2-1.441I$ .314	.383	.509	27.1	36.0
54	.809	.655	.588	1.132	.3235	$1.654I^2-1.455I$ .314	.379	.501	25.7	34.0
56	.830	.688	.560	1.160	.308	$1.688I^2-1.468I$ .314	.379	.491	24.4	31.6
58	.848	.719	.530	1.188	.2915	$1.719I^2-1.480I$ .314	.383	.478	23.4	29.2
60	.866	.750	.500	1.21	.275	$1.750I^2-1.485I$ .314	Imaginary		--	--

Solution of $I^2 + I^2\sin^2\theta - 1.4I\sin\theta - .55I\cos\theta + .314 = 0$

Table V

θ	2a	b	b^2	c	2ac	4ac	b^2-4ac	$\sqrt{b^2-4ac}$	$-b+\sqrt{\ }$	$-b-\sqrt{\ }$	I Root 1	I Root 2
42	2.90	-1.35	1.81	.314	.91	1.82	-.005	Imaginary		--	--	--
44	2.96	-1.37	1.87	.314	.93	1.86	.009	.095	1.46	1.27	.493	.428
46	3.04	-1.39	1.84	.314	.95	1.91	.027	.164	1.56	1.23	.510	.405
48	3.10	-1.41	1.98	.314	.98	1.95	.032	.179	1.59	1.23	.512	.395
50	3.17	-1.42	2.03	.314	1.00	1.99	.038	.195	1.62	1.23	.511	.388
52	3.24	-1.44	2.08	.314	1.02	2.04	.042	.205	1.65	1.24	.509	.383
54	3.31	-1.46	2.12	.314	1.04	2.08	.042	.205	1.66	1.25	.501	.379
56	3.76	-1.47	2.16	.314	1.06	2.12	.037	.192	1.66	1.28	.491	.379
58	3.44	-1.48	2.19	.314	1.08	2.16	.027	.164	1.64	1.32	.478	.383
60	3.50	-1.49	2.21	.314	1.10	2.20	.012	.110	1.60	1.37	.457	.392
62	3.77	-1.49	2.23	.314	1.18	2.36	-.134	Imaginary		--	--	--

Solution of $I = \frac{-b \pm \sqrt{b^2 - 4ac}}{2a}$

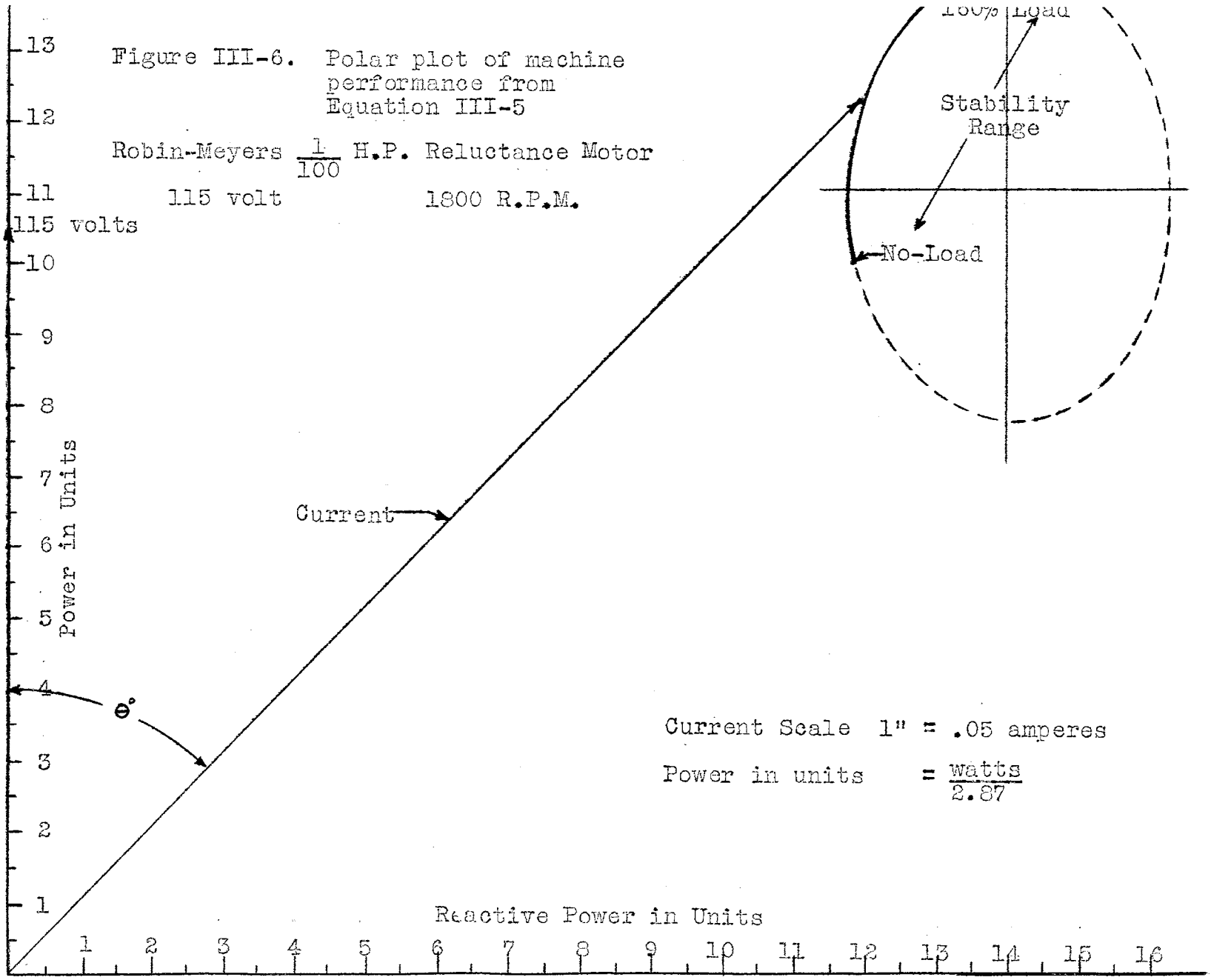
Figure III-6. Polar plot of machine performance from Equation III-5
Robin-Meyers 1/100 H.P. Reluctance Motor
115 volt 1800 R.P.M.
115 volts
Power in Units
Reactive Power in Units
Current
θ°
Stability Range
No-Load
Current Scale 1" = .05 amperes
Power in units = watts / 2.87

Calculation of Losses From Equation III-16

$$P_t = - .36\ P_o + .493\ \epsilon^{.203\ P_o} + P_c'$$

Table VI

P_c'	P_o	$- .36\ P_o$	$\epsilon^{.203\ P_o}$	$.493\epsilon^{.203\ P_o}$	P_t
28.507	0	0	1.00	.493	29.00
"	1	- .36	1.23	.607	28.75
"	2	- .72	1.50	.740	28.53
"	3	-1.08	1.84	.907	28.33
"	4	-1.44	2.25	1.10	28.17
"	5	-1.80	2.76	1.36	28.07
"	6	-2.16	3.38	1.67	28.02
"	7	-2.52	4.14	2.04	28.03
"	8	-2.88	5.07	2.50	28.13
"	9	-3.25	6.21	3.06	28.32
"	10	-3.60	7.62	2.76	28.67
"	11	-3.96	9.34	4.60	29.15
"	12	-4.32	11.44	5.64	29.83

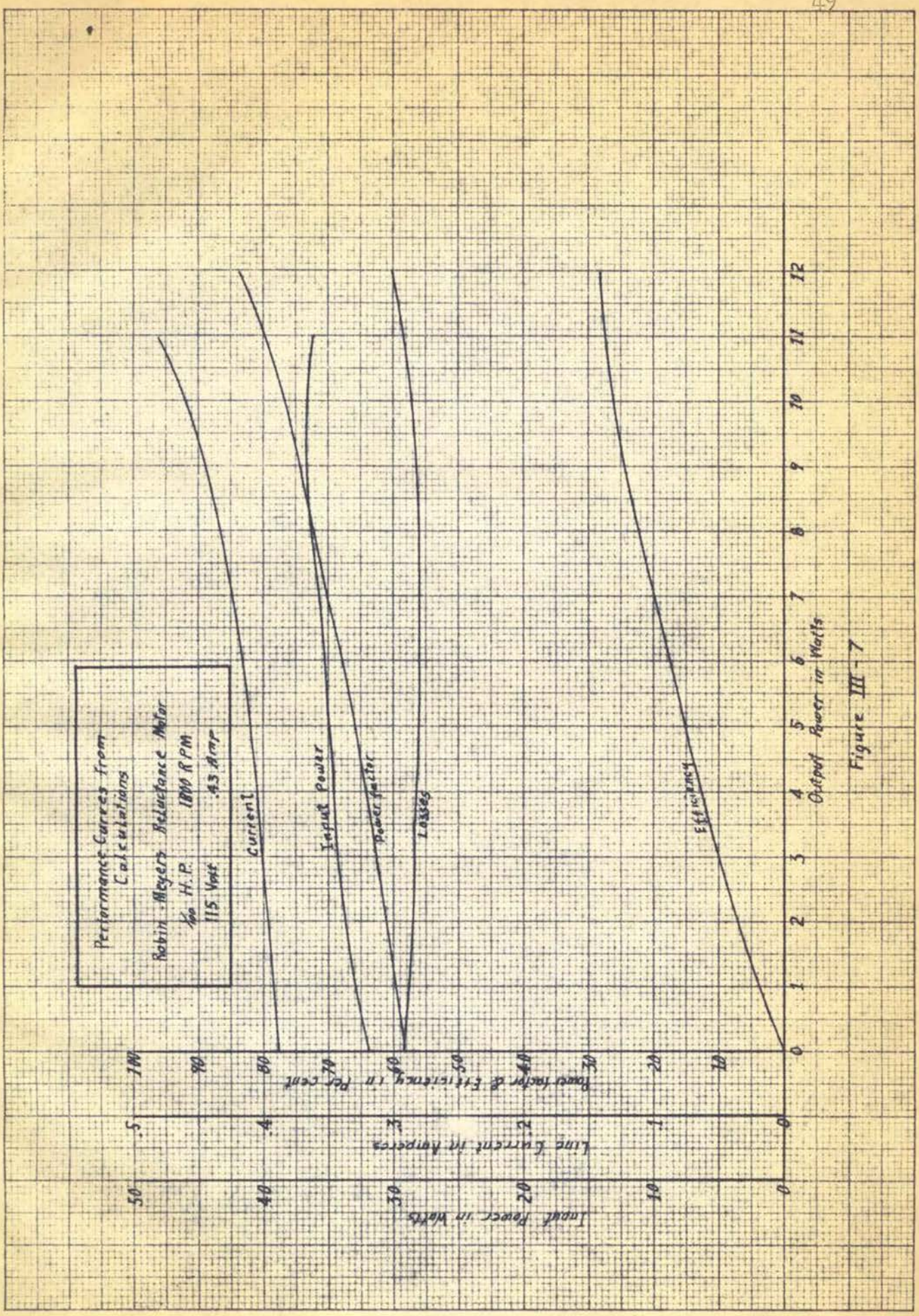
Performance Curves from Calculations
Robin-Meyers Reluctance Motor
1/20 H.P. 1800 RPM
115 Volt .43 Amp
Current
Input Power
Power factor
Losses
Efficiency
Output Power in Watts
Power Factor & Efficiency in Per cent
Line Current in Amperes
Input Power in Watts

Figure III-7

SUMMARIZATION

It seems worth while to summarize the procedure used in arriving at the characteristics of Figure III-7.

1. Losses versus output characteristic, (Figure III-7), from equation III-16.

2. Input curve, (Figure III-7), from losses plus output.

3. Current versus impedance angle, (Figure III-6), from equation III-5.

4. Current versus output as follows:
   a. Enter Figure III-7 with desired output point and read input watts.
   b. Convert input watts to power in units and enter Figure III-6 to find the corresponding current point.
   c. Scale the current magnitude.

5. Power-factor versus output as follows:
   a. Corresponding to the current point of 4-b above, read Reactive Power and Power in unit measure.
   b. Tan θ = Reactive Power/Power.
   c. Power-factor = Cos θ.

6. Efficiency = Output/Input.

CHAPTER IV

Approximate Circuit Diagram Method

The test data and the analysis of Chapter III suggest the circuit diagram of Figure IV-1 as an approximation for the machine under consideration.

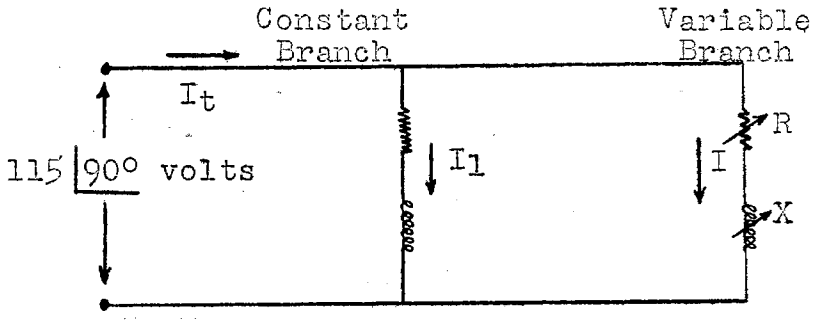

Figure IV-1. Approximate circuit diagram of single-phase reluctance motor.

The diagram consists of a constant branch and a variable branch in parallel on the 115 volt line. The reference direction for vectors is voltage at 90° to be consistent with the vector diagrams of Figures III-2 and III-6. Let the current taken by the constant branch be I_1 as shown in Figures IV-1 and IV-2. From the diagram of Figure III-2 this current is $.402\angle 43°$ amperes. The variable branch contains a variable resistor to account for changes of energy consumption with changes of load and a variable reactance to account for changes of reluctance. (See page 25). Since the current taken by the variable branch follows an elliptical path a very interesting possibility presents itself. Suppose a transformation of coordinates be effected such that the loci of current vectors taken by the

variable branch, when plotted in the transformed system, traces a circular pattern rather than an elliptical one. Such a trans-

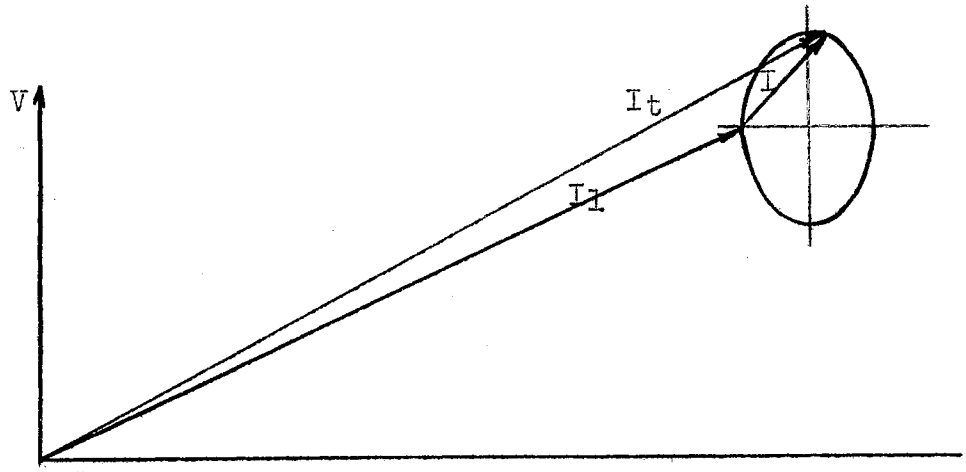

Figure IV-2. Vector diagram for the approximate circuit diagram of single-phase reluctance motor.

formation is possible because both the circle and the ellipse are conic sections. The advantages of the method will be apparent after a consideration of the mechanics of transformation.

Figure IV-3 shows the actual vector diagram of the variable branch in a plane behind that of the paper. The angle, φ, between the planes is the arc cosine $\frac{ad}{ab}$. This is apparent from the figure. The values of ad and ab may be obtained from Figure III-2.

$$\varphi = \text{Cos}^{-1} \frac{ad}{ab} = \text{Cos}^{-1} \frac{5.7}{8.2} \qquad \text{(IV-1)}$$

$$\varphi = 46^{\circ}$$

The reference vector, J V, has a corresponding vector in the transformed diagram designated as $\mathcal{J}V'$. They are related by the following:

$$\left| J\ V \right|_{mag} = \left| \mathcal{J} \frac{V'}{\text{Cos}\varphi} \right|_{mag}$$

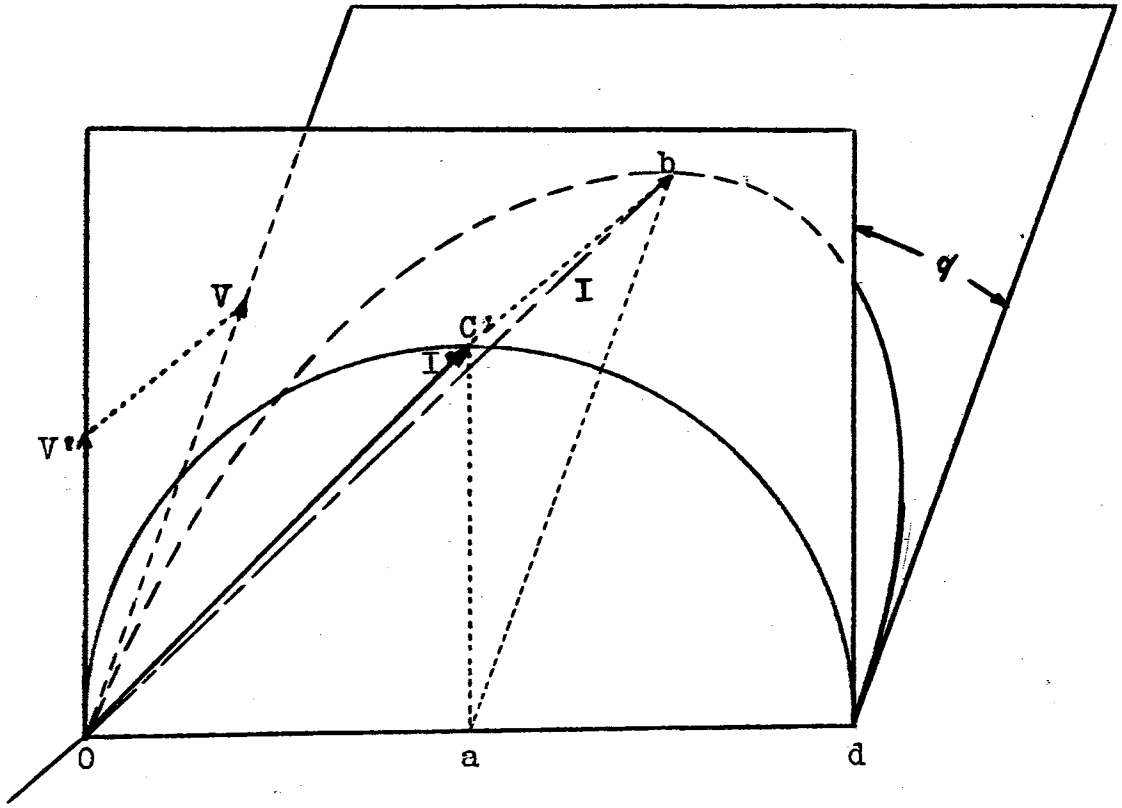

Figure IV-3. Vector diagram of the variable branch showing the actual and transformed views.

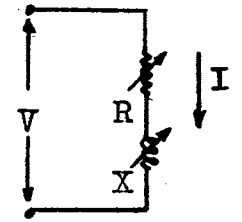

Figure IV-4. Circuit diagram of actual variable branch.

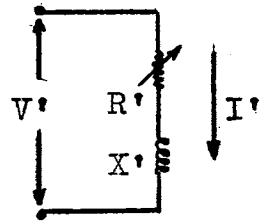

Figure IV-5. Circuit diagram of transformed variable branch.

$$115 = \frac{80}{.695}$$

The operator, J, will hereafter be understood to direct the vertical components on the actual diagram and the operator, $\jmath$, to direct the vertical components on the transformed diagram. To illustrate, the actual current, I, may be expressed as

$$I = \underline{oa} + J\ \underline{ab}$$

and the current I' as

$$I' = \underline{oa} + \jmath\ \underline{ac}$$

Now it may be seen that the horizontal components of any current, I, and the corresponding current, I', are the same. The vertical components are related in magnitude always by

$$\left| I \right|_{J\text{-comp}} = \left| \frac{I'}{\cos\varphi} \right|_{\jmath\text{-comp}} = 1.44 \left| I' \right|_{\jmath\text{-comp}} \qquad \text{(IV-2)}$$

A comparison of Figures IV-4 and IV-5 reveals the advantage of the transformation. The circuit diagram of the transformed branch contains only one variable parameter. The variation of I', and from it the variation of the actual current, I, may be easily calculated. The following procedure is suggested.

The voltage impressed on the transformed circuit is

$$\jmath V' = \jmath 115 \cos\varphi = \jmath 80 \text{ volts}$$

X' may be evaluated by making R' equal to zero. The current I' under this condition is the diameter of the semi-circle and from Figure III-2 is:

$$I' = .115 + \jmath 0 \text{ amps}$$

$$X' = \frac{80}{.115} = 695 \text{ ohms}$$

In general

$$I' = \frac{\jmath V'}{R' + \jmath X'} = \frac{\jmath V'(R' - \jmath X')}{R'^2 + X'^2}$$

$$I' = \frac{V' X'}{R'^2 + X'^2} + J \frac{V' R'}{R'^2 + X'^2} \qquad \text{(IV-3)}$$

Making use of the relationship given by equation IV-2 an equation for the current to the actual equivalent branch may be written.

$$I = \frac{V' X'}{R'^2 + X'^2} \pm J \frac{1.44\, V'R'}{R'^2 + X'^2} \qquad \text{(IV-4)}$$

The total current to the equivalent circuit is

$$\begin{aligned} I_t &= I_1 + I \\ &= .402 \angle 43^\circ + \frac{80 \times 695}{R'^2 + 695^2} \pm J \frac{1.44 \times 80R'}{R'^2 + 695^2} \\ &= \left(.295 + \frac{55600}{R'^2 + 695^2}\right) + J \left(.275 \pm \frac{115\, R'}{R'^2 + 695^2}\right) \end{aligned} \qquad \text{(IV-5)}$$

A number of values of I_t have been calculated making use of Table VII. The elliptical plot of Figure III-6 may be accomplished from this table as well as from Table V, and the calculation of the former is a great deal less difficult. The $\pm$ term in equations IV-4 and IV-5 should not be disturbing. It arises from the mathematical translation of coordinates. The complex number, $3 + J2$, may be expressed as $3 + J4 - J2$ if for some reason it is more convenient. No physical significance need be attached.

No attempt is made to identify the two branches of Figure IV-1 with actual circuits of the machine. The equivalent circuit developed here is merely recognized as the least complicated combination of parameters possible to draw from the line the currents taken by the motor of this study.

Table VII

$R'x10^{-2}$	R'^2x10^{-4}	$\frac{55600}{R'^2+695^2}$	$\frac{+115\,R'}{R'^2+695^2}$	$\lvert I \rvert_{REAL}$	$\lvert I \rvert_{IMAG}$	It	θ
∞	∞	0	0	.295	.275 .275	.402 .402	43° 43°
20	400	.012	.051	.308	.224 .326	.382 .444	54.2 43.4
18	324	.015	.056	.310	.219 .331	.375 .445	54.7 43.2
16	256	.018	.061	.313	.215 .336	.380 .465	55.6 43.1
14	196	.023	.066	.318	.209 .341	.380 .465	56.7 43.1
12	144	.029	.072	.324	.203 .347	.383 .475	57.9 42.9
10	100	.037	.077	.332	.198 .352	.387 .487	59.2 43.0
9	81	.043	.080	.338	.195 .355	.392 .492	60.2 43.5
8	64	.050	.082	.345	.193 .357	.395 .496	60.8 44.0
7	49	.057	.083	.352	.192 .358	.400 .500	61.4 44.6
6	36	.066	.082	.361	.192 .357	.408 .507	61.9 45.3
5	25	.076	.079	.371	.197 .353	.420 .510	62.0 46.4
4	16	.087	.072	.384	.203 .347	.430 .515	61.8 47.7
3	9	.097	.060	.392	.215 .335	.445 .515	61.0 49.5
2	4	.107	.044	.402	.231 .329	.462 .514	60.0 50.0
1	1	.113	.023	.408	.252 .298	.475 .505	58.1 53.9
0	0	.115	0	.410	.275 .275	.493 .493	56.2 56.2

CONCLUSIONS

It is believed that this thesis is the most extensive analysis of the single-phase reluctance motor available. Some literature dealing with the three-phase reluctance motor in large sizes can be found, and many authors of A. C. machinery texts mention the presence of reluctance power in salient-pole synchronous motors, but the analysis of the single-phase motor presented in this work is original and believed to be quite singular.

Prominent among the revelations of the study is the extreme importance played by the selection of magnetic materials upon the performance of the motor. This is an item of consideration for all rotating electrical machinery, but for the motor of this study adjustment of rotor design can be effected only by changing the shape of the punchings or by changing the material itself. The ideal rotor would incorporate an optimum of these two features.

It was observed that the loci of current vectors plot an elliptical path as load is added. The only conclusions that one can reach from this observation is that the overall reactance of the machine changes with changes of load. This is a logical conclusion, since the salient-pole rotor changes position with respect to the rotating field each time load is changed. Langsdorf, in his Theory of Alternating Current Machinery,[1] substantiates this idea by developing for the three-phase

---

[1] Alexander S. Langsdorf, Theory of Alternating Current Machinery, p. 448.

synchronous motor an expression for equivalent impedance which may be identified with the equation of an ellipse.

The equation for losses as a function of output developed in Chapter III is recognized as empirical in nature. The exact form of the equation would, therefore, be different for another motor, but the method is unique and the general approach applicable to all similar machines. The entire method of performance calculations as presented in this thesis is intended for use where a test machine is available. This is typical procedure in small motor design.

It is believed that further research will reveal more definite physical explanations for the empirical constants employed in the method presented here, and it is hoped that this work will pave the way for such research.

BIBLIOGRAPHY

Boast, W. B. Principles of Electric and Magnetic Fields. New York: Harper Publishing Company, 1948.

Bozarth, R. M. "Present Status of Ferromagnetic Theory." Transactions of American Institute of Electrical Engineers, 54 (November, 1935), 1251.

Electrical Engineering Staff, M.I.T. Magnetic Circuits and Transformers. New York: John Wiley and Sons, 1943.

Hart, W. L., Wilson, W. A., and Tracey, J. I. College Mathematics. Boston: D. C. Heath and Company, 1943.

Langsdorf, A. S. Theory of Alternating-Current Machinery. New York: McGraw-Hill Book Company, 1937.

McFarland, T. C. Alternating-Current Machines. New York: D. Van Nostrand Company, 1948.

Puchstein, A. F. and Lloyd, T. C. Alternating-Current Machines. New York: John Wiley and Sons, 1942.

Ricker, C. W. and Tucker, C. E. Electrical Engineering Laboratory Experiments. New York: McGraw-Hill Book Company, 1940.

Rotors, H. C. Electromagnetic Devices. New York: John Wiley and Sons, 1941.

Shoults, D. R., Rife, C. J., and Johnson, T. C. Electric Motors in Industry. New York: John Wiley and Sons, 1942.

Skilling, H. H. Fundamentals of Electric Waves. New York: John Wiley and Sons, 1948.

Trickey, P. H. "Performance Calculations on Polyphase Reluctance Motors." Transactions of American Institute of Electrical Engineers, 65 (April, 1946), 191.

Veinott, C. G. Fractional Horsepower Electric Motors. New York: McGraw-Hill Book Company, 1939.

- Patty McAffrey Howell -